An imaged-based inverse finite element method to determine *in-vivo* mechanical properties of the human trabecular meshwork

Anup D. Pant[1], Larry Kagemann[2,3,*], Joel S. Schuman[3], Ian A. Sigal[4], Rouzbeh Amini[1]

[1]Department of Biomedical Engineering, The University of Akron, Akron, OH, USA; [2]Lead Reviewer and Biomedical Engineer, Division of Ophthalmic and ENT Devices, Office of Device Evaluation, Center for Devices and Radiological Health, Food and Drug Administration, Silver Spring, MD, USA; [3]Department of Ophthalmology, NYU School of Medicine and Langone Medical Center, New York, NY, USA; [4]Department of Ophthalmology, The University of Pittsburgh, Pittsburgh, PA, USA

Abstract

Aim: Previous studies have shown that the trabecular meshwork (TM) is mechanically stiffer in glaucomatous eyes as compared to normal eyes. It is believed that elevated TM stiffness increases resistance to the aqueous humor outflow, producing increased intraocular pressure (IOP). It would be advantageous to measure TM mechanical properties *in vivo*, as these properties are believed to play an important role in the pathophysiology of glaucoma and could be useful for identifying potential risk factors. The purpose of this study was to develop a method to estimate *in-vivo* TM mechanical properties using clinically available exams and computer simulations.
Design: Inverse finite element simulation
Methods: A finite element model of the TM was constructed from optical coherence tomography (OCT) images of a healthy volunteer before and during IOP elevation. An axisymmetric model of the TM was then constructed. Images of the TM at a baseline IOP level of 11, and elevated level of 23 mmHg were treated as the undeformed and deformed configurations, respectively. An inverse modeling technique was subsequently used to estimate the TM shear modulus (G). An optimization technique was

*Dr. Kagemann's contributions are independent of his work with the FDA. The data and opinions expressed herein do not represent those of any regulatory agency.

Correspondence: Rouzbeh Amini, Olson Research Center Room 301F, 260 S Forge St., Akron, Ohio 44325, USA.
E-mail: ramini@uakron.edu

used to find the shear modulus that minimized the difference between Schlemm's canal area in the *in-vivo* images and simulations.

Results: Upon completion of inverse finite element modeling, the simulated area of the Schlemm's canal changed from 8,889 μm^2 to 2,088 μm^2, similar to the experimentally measured areal change of the canal (from 8,889 μm^2 to 2,100 μm^2). The calculated value of shear modulus was found to be 1.93 kPa, (implying an approximate Young's modulus of 5.75 kPa), which is consistent with previous *ex-vivo* measurements.

Conclusion: The combined imaging and computational simulation technique provides a unique approach to calculate the mechanical properties of the TM *in vivo* without any surgical intervention. Quantification of such mechanical properties will help us examine the mechanistic role of TM biomechanics in the regulation of IOP in healthy and glaucomatous eyes.

Keywords: Inverse algorithm, glaucoma, intraocular pressure (IOP), Schlemm's canal, trabecular meshwork

1. Introduction

Glaucoma is a major health concern and a leading cause of blindness, affecting more than 3 million people in the US and 63 million people worldwide.[1,2] Globally, the number of glaucomatous bilateral blindness cases is expected to exceed 11 million by 2020;[3] it has been estimated that, by 2040, 111.8 million people will have glaucoma worldwide.[1] Glaucoma is the cause of blindness for 120,000 people in the US, accounting for 9–12% of all cases of blindness.[3,4] Elevated intraocular pressure (IOP), a risk factor for glaucoma, could be caused by increased resistance to the outflow of aqueous humor. Aqueous humor exits the anterior eye through two pathways: the trabecular meshwork (TM) pathway, accounting for ~60% of the outflow, and the uveoscleral pathway.[5] The TM pathway begins at the apex of the iridocorneal angle. It continues through the trabecular tissue, across the inner wall of Schlemm's canal, into the canal's lumen, and into the collector channels. This pathway ultimately leads the aqueous humor to the episcleral venous circulation.[6] IOP increases with respect to normal conditions both if the resistance to aqueous outflow or the aqueous production rate increases.

The TM comprises three different layers: the innermost portion of the TM (the iridic and uveal areas), the central corneoscleral part (which lies between the cornea and scleral spur), and the outermost juxtacanalicular (JXT) part or cribriform layer (which lies between the corneoscleral layer and the inner wall of Schlemm's canal).[7] Different studies have attributed the outermost JXT layer as the site of the outflow resistance.[8,9] The endothelial cells contained in the JXT tissue outer region lines the inner wall of Schlemm's canal, an oval shaped structure that collects aqueous humor.

The extracellular matrix (ECM) of the various layers of the TM consists of a number of components such as collagen fibrils, elastic fibers, microfibril, and sheath-derived materials along with basement membrane proteins, type IV collagen, laminin, proteoglycans, and glycosaminoglycans.[10] In glaucomatous eyes, significant changes in the components comprising the ECM and in TM cells have been identified. Three examples of such changes in the TM at the cellular/ECM level are listed below:

1. Primary open-angle glaucoma (POAG) is associated with an excessive accumulation of sheath-derived plaques in the TM in comparison to the normal eye.[11]
2. In steroid-induced glaucoma, the accumulation of the extra cellular materials has shown to be present; however, unlike POAG, the material was found to be in a fingerprint-like morphology that resembled basement membranes throughout all layers of the TM.[12]
3. In pigmentary glaucoma, TM cell loss has been found to be prominent.[13,14] In addition to the trabecular cells loss, Gottanka *et al.* found other distinctive changes including trabecular lamellae fusion, collapse of the intertrabecular space, increase in extracellular material, and canal obliteration in eyes suffering from pigmentary glaucoma.[13]

It is also noteworthy that the cellularity of the TM decreases with age, a known risk factor for glaucoma.[15,16] These changes in the TM at the cellular/ECM level may affect its tissue-level mechanical properties. Since tissue-level mechanical properties are parameters that can be quantified using standard bench-top methods, they are a good candidate for comparative studies between normal and glaucomatous tissues. In particular, previous studies have attributed the stiffness of the TM as an indicator for glaucoma. For instance, Last *et al.*[17] found TM stiffness to be considerably higher in POAG eyes compared to that of normal eyes. They hypothesized that the underlying cause for the higher stiffness value in glaucomatous eyes, *i.e.*, the TM changes at the cellular/ECM level, contributed to the decreased permeability of the TM to the aqueous humor outflow. Similarly, Russel *et al.*[18] observed that glaucomatous TM cells were significantly stiffer than those in a normal TM.

The above studies clearly show an important correlation between glaucoma and increased TM stiffness. All these studies, however, are limited in application, as they have been conducted using isolated tissue samples. Specifically, previous studies in other tissues have shown that mechanical loading and calculated mechanical properties could be significantly different in the *in-vivo* and *ex-vivo* environments.[19] In addition, using *ex-vivo* samples significantly limits the applicability of the measurement as a diagnostic tool in the future. To bridge this knowledge gap, we propose a new method to determine the mechanical properties of the TM *in vivo* without the need for any surgical intervention by employing computer simulations and clinically available non-invasive TM imaging techniques.
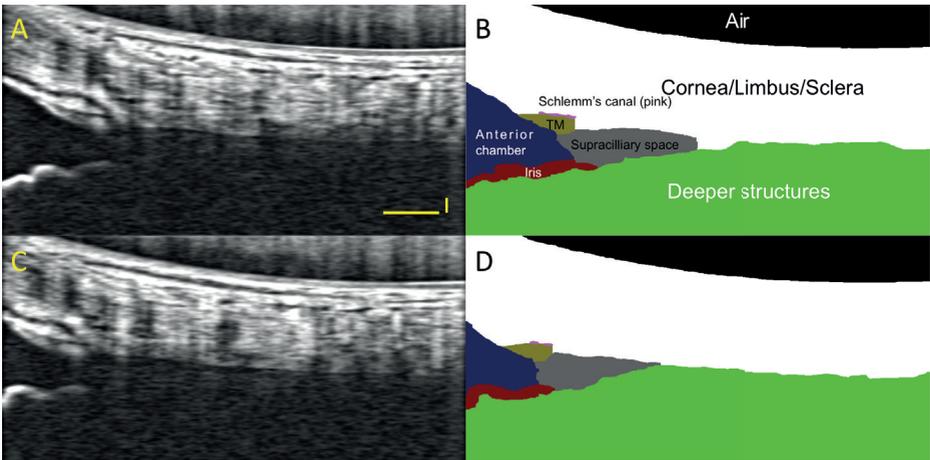
Fig 1. (*A*) B-scan and (*B*) segmented images of the TM at baseline IOP, and (*C*) B-scan and (*D*) segmented images of the TM at elevated IOP. Scale bars are 250 µm (horizontal and vertical scale bars are of different length as the scans have a different aspect ratio).

2. Methods

2.1. Imaging and segmentation

The temporal limbus of a healthy subject (female, age 26 years) was imaged using optical coherence tomography (OCT, Cirrus, Zeiss, Dublin, CA) at baseline and during IOP elevation. IOP was elevated using an ophthalmodynamometer (Bailliart ophthalmodynamometer, W. Koch Optik, Zurich, Switzerland) applying a 10-g force to the sclera. IOP was also measured at baseline and during IOP elevation by Goldmann applanation tonometry. The tip of the ophthalmodynamometer was placed temporal to the cornea, midway between the limbus and lateral canthus. A team of three researchers, one operating the OCT or Goldmann applanation tonometer, one applying pressure to the sclera, and one assisting the patient with head placement in the headrest, was used. The corresponding locations on the Schlemm's canal were identified in radial OCT cross-sectional B-scans based on the pattern of the limbal vessel crossings.[20] The images were segmented manually using the GNU Image Manipulation Program (GIMP 2.8.14) into air, cornea/limbus/sclera complex, Schlemm's canal, TM, anterior chamber, iris, supracilliary space, and "deeper structures" (those beyond the limit of penetration of the OCT scan) (Fig. 1).

2.2. Governing equation

An axisymmetric model of the TM was constructed, similar to our previous finite element models of the anterior eye.[21-24] The TM was modeled as a neo-Hookean solid material. The governing stress balance equation is given by:

$$\nabla . \boldsymbol{\sigma} = 0 \tag{1}$$

where $\boldsymbol{\sigma}$ represented the Cauchy stress tensor:

$$\boldsymbol{\sigma} = \frac{G}{\det \mathbf{F}} (\mathbf{B} - \mathbf{I}) + \frac{2Gv}{(1 - 2v) \det \mathbf{F}} \ln(\det \mathbf{F}) \, \mathbf{I} \tag{2}$$

where G was the shear modulus, v was the Poisson's ratio, $\mathbf{I}$ was the identity tensor, $\mathbf{F}$ was the deformation gradient tensor, and $\mathbf{B}$ was the left Cauchy–Green deformation tensor. The tensors $\mathbf{F}$ and $\mathbf{B}$ were defined as:

$$\mathbf{F} = \frac{d\mathbf{x}}{d\mathbf{X}} \tag{3}$$

$$\mathbf{B} = \mathbf{F}\mathbf{F}^{\mathsf{T}}, \tag{4}$$

where $\mathbf{x}$ was the current position of a material point and $\mathbf{X}$ was its resting position.

2.3. Meshing

The finite element meshes were generated based on TM geometry segmented from *in-vivo* images according to the following steps:

1. The segmented TM images with the appropriate aspect ratio (Fig. 2A) were imported in SolidWorks (Dassault Systèmes, Velizy-Villacoublay, France) and the boundaries of the TM section were manually tracked and obtained (Fig. 2B).
2. The SolidWorks output file was then imported into Abaqus (Dassault Systèmes, Velizy-Villacoublay, France) and meshed using a paving approach (Fig. 2C).
3. As Abaqus was capable of generating only 8-node quadrilateral elements, the output of the Abaqus mesh was subsequently imported into an internally developed C code, which was used to add an extra node to the elements to generate 9-node bi-quadratic quadrilateral finite elements.

The 9-node bi-quadratic quadrilateral elements were subsequently used in our internally developed inverse finite element code, as described in the next section.

2.4. Inverse finite element modeling

A pressure boundary condition with the constant value of IOP was applied along the boundary elements of the TM domain facing the iridocorneal angle (shown by solid arrows in Fig. 3C). The pressure boundary condition was applied to mimic the changes in the IOP *in-vivo*. In particular, since the IOP of the undeformed configuration was 11 mmHg and the IOP of the deformed configuration was 23 mmHg, the difference of 12 mmHg was applied as the pressure boundary condition. The TM boundaries that connect it to the much stiffer surrounding tissues (Fig. 3C) were
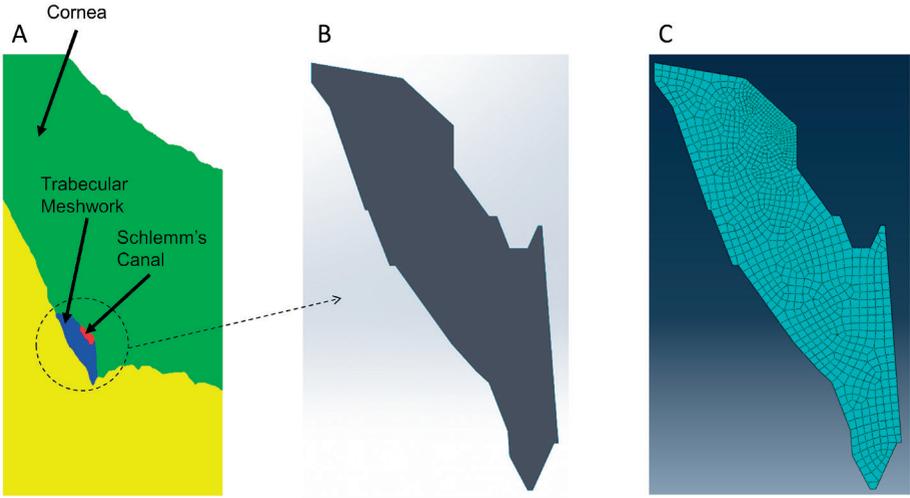
Fig 2. (*A*) A segmented image of the TM. (*B*) TM image imported to SolidWorks (Dassault Systèmes, Velizy-Villacoublay, France) to generate the coordinates of the TM boundaries. (*C*) Finite element meshes generated using Abaqus (Dassault Systèmes, Velizy-Villacoublay, France).
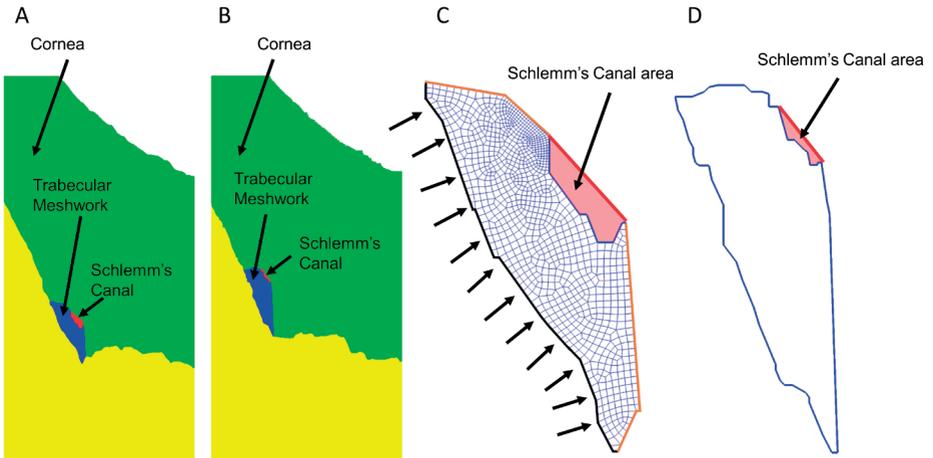

Fig 3. Segmented images of the trabecular meshwork in (*A*) undeformed and (*B*) deformed configuration. Finite element mesh and boundary of the trabecular meshwork in (*C*) undeformed and in (*D*) deformed configuration, respectively. The boundary of the deformed configuration is provided only for identifying the Schlemm's canal area. In (*C*) the orange lines represent the fixed boundary condition, whereas the black edge represents the region where the pressure was applied.

assumed to have negligible deformation in comparison to the rest of the tissue. Thus, a fixed boundary condition was chosen for these regions. An additional contact stress, $\boldsymbol{\sigma}_{contact}$, was applied along the boundary of Schlemm's canal to prevent tissue penetration into the stiffer scleral tissue:

$$\boldsymbol{\sigma}_{contact} = A\, e^{\frac{d}{E}}\, \mathbf{n} \otimes n \tag{5}$$

where d is the shortest distance between the TM and the sclera, A and E are adjustable coefficients, $\mathbf{n}$ is the normal vector to the boundary, and $\otimes$ is the dyadic operator.

We then used an inverse modeling approach[25] to calculate the shear modulus G from the experimental deformation data using a differential algorithm. The material was assumed to be nearly incompressible, so a Poisson's ratio (v) of 0.49 was used. The basic overview of the process is given in the flowchart shown in Figure 4. The objective function was defined as absolute value of the difference between the Schlemm's canal area of the experimental measurements SC_{exp} (the shaded area in Fig. 3D) and the genetically driven finite element solution SC_{sim} (the shaded area in Fig. 3C after the deformation is applied):
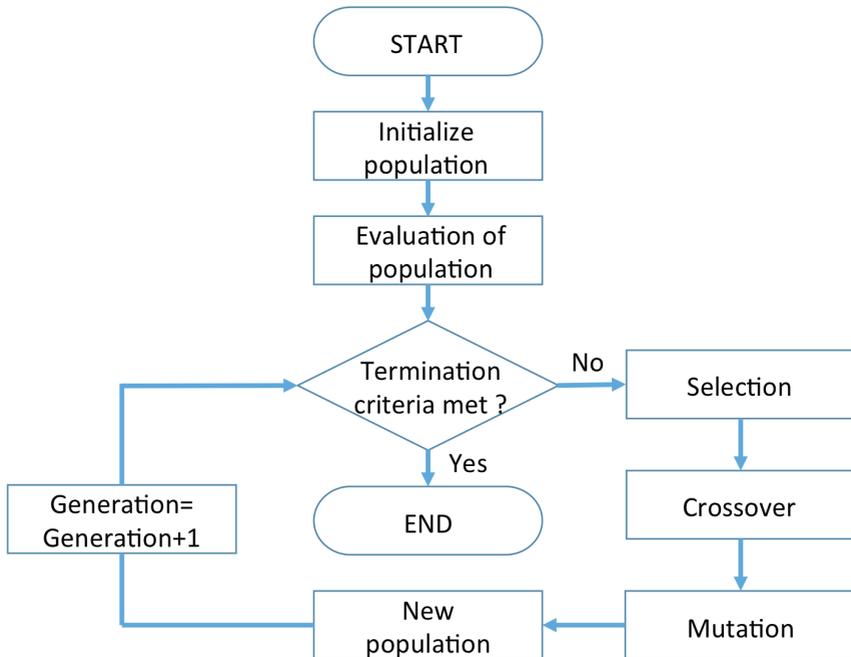

Fig 4. Inverse algorithm flowchart.

$$\text{Error} = |SC_{exp} - SC_{sim}| \qquad (6)$$

The initial guesses for G were chosen between 10 kPa and 90 kPa. The simulations were performed using an HP Intel Xeon machine at the Ohio Supercomputer Center (Columbus, OH, USA).[26] The inverse algorithm ran for 50 generations to ensure the convergence of the solution.

3. Results

From the optimization technique, a value of 1.93 kPa was obtained for the TM shear modulus, G. The simulated area of the Schlemm's canal was found to be ~2,088 μm^2 (the area of the undeformed configuration was ~8,889 um^2) whereas the area of the experimental image was found to be ~2,100 μm^2. Figure 5 shows the simulated result of TM using a shear modulus of 1.93 kPa (a) without and (b) with the application of a contact force. The optimization convergence was independent of our initial guesses, and the broader ranges of initial guesses only increased the computational time. On average, the solution process took approximately 300 minutes (for 50 generations, the number of iterations for optimizing G).
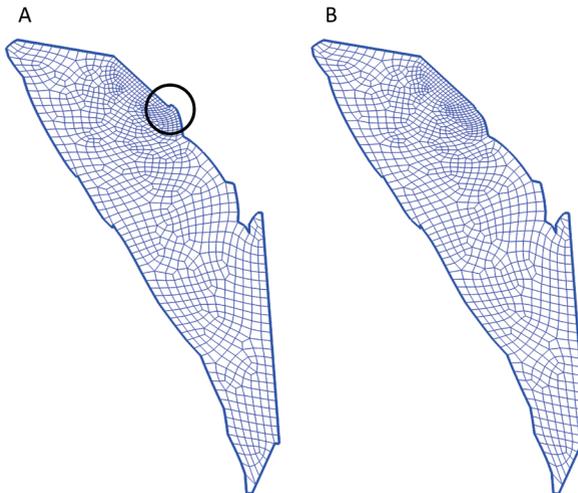

Fig 5. Simulated results of the deformation of the TM (A) without the application of contact force (the marked circle denotes the penetration of the TM into the stiffer scleral tissue) and (B) with the application of contact force.

4. Discussion

The best estimation of compressive Young's modulus of elasticity (E) was obtained in a study by Last *et al.*, with an atomic force microscopy measurement of dissected TM tissues.[18] They found that TM tissue from a non-glaucomatous donor eye had a modulus of elasticity of approximately 4 kPa. In our study in a living eye, we found a shear modulus value of 1.93 kPa, which is approximately equivalent to an elastic modulus of 5.75 kPa. Similarly, the use of the additional contact force did not have a dramatic effect on the optimized value of the shear modulus, and *G* was found to be 2.0 kPa (~4% different from 1.93 kPa) when the contact force was not applied. Our measurement in the living eye was only slightly larger than that of excised tissues.

Using simplified beam theory, Johnson *et al.* estimated the TM elastic modulus to be 128 kPa (approximately equivalent to a shear modulus value of 43 kPa), which is substantially higher than our estimated value.[27] The simplified geometry and material models used in the study of Johnson and colleagues could have contributed to the different outcomes: we used a nearly incompressible neo-Hookean solid as our material model, whereas they employed a linear elastic material model. In addition, we did not simplify the TM deformation to a beam bending model. Camras *et al.*, using uniaxial stretching experiments, found the circumferential elastic modulus of a normal TM to be 51.5 ± 13.6 MPa[28] and that of a glaucomatous TM to be 17.5 ± 5.8 MPa.[15] Clearly, the reported modulus values in the literature span a large spectrum, with a difference of nearly three orders of magnitude. One reason for such discrepancy could be the way of measuring the stiffness. Camras *et al.* measured the axial stiffness using larger tissue strips, whereas Last *et al.* only measured the local compressive stiffness on a cellular level. It is noteworthy that, none of these *ex-vivo* methods accurately encompass the mechanical response of the TM *in vivo*. In this study, we attempted to capture the *in-vivo* response of the TM at a tissue level. Another reason could be the difference between cadaveric eyes used in the conventional testing methods and our measurements *in vivo*. Nonetheless, more research is needed to increase the number of experimental fittings both in multiple levels of IOP measurements and among additional volunteers using our technique. Using a wider range of samples will help us discern the interplay of the mechanical properties of the TM and regulation of IOP in healthy and glaucomatous eyes. More detailed studies to identify the differences between the TM of normal and glaucoma subjects by testing a sufficient number of cases so as to allow a suitable statistical analysis are necessary.

In the realm of biomechanics, most soft tissues are treated as incompress-ible (or nearly incompressible) materials since they consist largely of water.[29] However, when there is a fluid motion within the tissue, more complex constitutive models, involving mixture or poroelasticity theory, are available to account for the fluid-solid interaction.[30-32] Implementation of such complex models in the inverse finite element analysis of TM deformation requires more than one fitting parameter.

Increasing the number of fitting parameters could jeopardize the uniqueness of the solution. As such, in the current study, we opted to use a more generalized nearly incompressible model to simulate the deformation of the TM, and we employed only the shear modulus as our fitting parameter. We have previously used smaller values of Poisson's ratio as an indicator of compressibility in the simulation of iris deformation.[24] In our future studies, we aim to perform parametric studies using our finite element model and examine the influence of TM compressibility on the calculated value of the shear modulus. In addition, inverse finite element modeling using both the shear modulus and Poisson's ratio as the fitting parameters can be performed, if necessary.

In inverse modeling of complex geometries, the choice of objective functions can affect the quality of the fitting process.[33] In our study, the Schlemm's canal boundary was detected with a high level of confidence. As such, the experimental errors due to segmentation were minimized with the choice of Schlemm's canal area as the objective function. In addition, changes in the Schlemm's canal area corresponded to lateral deformation of the TM. Segmentation of the TM from the surrounding tissues is not as trivial; consequently, change in the cross-sectional area of the TM was not used as an objective function in our current study. If future advances in medical imaging provide more reliable methods for detecting the boundary between the TM and the surrounding tissues, the fidelity of Schlemm's canal as the objective function in comparison to the other possible alternatives should be examined.

5. Conclusion

Our proposed technique provides a new approach to quantify the mechanical properties of the TM *in vivo* by using only clinical imaging and computer simulations without the need for any surgical intervention. Our technique could provide a framework for the development of future diagnostic techniques to detect glaucoma at its earlier stages and for assessment of treatment methods that could bring TM stiffness to its normal values.

Acknowledgement

References

1.   Tham Y, Li X, Wong TY, Quigley HA, Aung T, Cheng C. Global Prevalence of Glaucoma and Projections of Glaucoma Burden through 2040: A Systematic Review and Meta-Analysis. Ophthalmology 2014;121(11):2081-2090. Available from: http://linkinghub.elsevier.com/retrieve/pii/S0161642014004333 doi: 10.1016/j.ophtha.2014.05.013.
2.   Grant WM, Burke JF. Why do some people go blind from glaucoma. Ophthalmology 1982;89(9):991-998. Available from: http://linkinghub.elsevier.com/retrieve/pii/S0161642082346758 doi: 10.1016/S0161-6420(82)34675-8.
3.   Quigley HA, Broman AT. The number of people with glaucoma worldwide in 2010 and 2020. Br J Ophthalmol 2006;90(3):262-267. Available from: http://bjo.bmj.com/cgi/doi/10.1136/bjo.2005.081224 doi: 10.1136/bjo.2005.081224.
4.   Congdon N, O'Colmain B, Klaver CC, Klein R, Munoz B, Friedman DS, et al. Causes and prevalence of visual impairment among adults in the United States. Arch Ophthalmol 2004;122(4):477-485. Available from: http://archopht.jamanetwork.com/article.aspx?doi=10.1001/archopht.122.4.477 doi: 10.1001/archopht.122.4.477.
5.   Alm A, Nilsson SF. Uveoscleral outflow–a review. Exp Eye Res 2009;88(4):760-768. Available from: http://linkinghub.elsevier.com/retrieve/pii/S0014483508004351 doi: 10.1016/j.exer.2008.12.012.
6.   Kaufman PL, Adler FH, Levin LA, Alm A. Adler's Physiology of the Eye. New York: Elsevier Health Sciences; 2011.
7.   Kahook MY, Schuman JS, Epstein DL. Chandler and Grant's Glaucoma. Thorofare, N.J. SLACK Incorporated; 2013.
8.   Rohen J, Witmer R. Electron microscopic studies on the trabecular meshwork in glaucoma simplex. Albrecht von Graefes Archiv für klinische und experimentelle Ophthalmologie 1972;183(4):251-266. Available from: http://link.springer.com/10.1007/BF00496153 doi: 10.1007/BF00496153.
9.   Mäepea O, Bill A. The pressures in the episcleral veins, Schlemm's canal and the trabecular meshwork in monkeys: effects of changes in intraocular pressure. Exp Eye Res 1989;49(4):645-663. Available from: http://linkinghub.elsevier.com/retrieve/pii/S0014483589800600 doi: 10.1016/S0014-4835(89)80060-0.
10. Acott TS, Kelley MJ. Extracellular matrix in the trabecular meshwork. Experimental Eye Research 2008;86(4):543-561. Available from: http://linkinghub.elsevier.com/retrieve/pii/S0014483508000171 doi: 10.1016/j.exer.2008.01.013.
11. Gottanka J, Johnson DH, Martus P, Lütjen-Drecoll E. Severity of optic nerve damage in eyes with POAG is correlated with changes in the trabecular meshwork. J Glaucoma 1997;6(2):123-132.
12. Johnson D, Flügel C, Hoffmann F, Futa R, Lütjen-Drecoll E. Ultrastructural changes in the trabecular meshwork of human eyes treated with corticosteroids. Arch Ophthalmol 1997;115(3):375-383. Available from: http://archopht.jamanetwork.com/article.aspx?doi=10.1001/archopht.1997.01100150377011 doi: 10.1001/archopht.1997.01100150377011. [Google Scholar]
13. Gottanka J, Johnson DH, Grehn F, Lütjen-Drecoll E. Histologic findings in pigment dispersion syndrome and pigmentary glaucoma. J Glaucoma 2006;15(2):142-151. Available from: http://content.wkhealth.com/linkback/openurl?sid=WKPTLP:landingpage&an=00061198-200604000-00011 doi: 10.1097/00061198-200604000-00011. [Google Scholar]
14. Murphy CG, Johnson M, Alvarado JA. Juxtacanalicular tissue in pigmentary and primary open angle glaucoma the hydrodynamic role of pigment and other constituents. Arch Ophthalmol 1992;110(12):1779-1785. Available from: http://archopht.jamanetwork.com/article.aspx?doi=10.1001/archopht.1992.01080240119043 doi: 10.1001/archopht.1992.01080240119043.
15. Camras LJ, Stamer WD, Epstein D, Gonzalez P, Yuan F. Circumferential tensile stiffness of glaucomatous trabecular meshwork. Invest Ophthalmol Vis Sci 2014;55(2):814-823. Available from: http://iovs.arvojournals.org/article.aspx?doi=10.1167/iovs.13-13091 doi: 10.1167/iovs.13-13091.
16. Alvarado J, Murphy C, Polansky J, Juster R. Age-related changes in trabecular meshwork cellularity. Invest Ophthalmol Vis Sci 1981;21(5):714-727.

17. Last JA, Pan T, Ding Y, Reilly CM, Keller K, Acott TS, et al. Elastic modulus determination of normal and glaucomatous human trabecular meshwork. Invest Ophthalmol Vis Sci 2011;52(5):2147-2152. Available from: http://iovs.arvojournals.org/article.aspx?doi=10.1167/iovs.10-6342 doi: 10.1167/iovs.10-6342.

18. Russell P, Last J, Ding Y, Pan T, Acott T, Keller K, et al. Compliance and the human trabecular meshwork: implications about glaucoma. Invest Ophthalmol Vis Sci 2010;51(13):3205-3205.

19. Brouwer I, Ustin J, Bentley L, Sherman A, Dhruv N, Tendick . Measuring in vivo animal soft tissue properties for haptic modeling in surgical. Medicine meets virtual reality.;2001:69-74.

20. Kagemann L, Wang B, Wollstein G, Ishikawa H, Nevins JE, Nadler Z, et al. IOP elevation reduces Schlemm's canal cross-sectional area. Invest Ophthalmol Vis Sci 2014;55(3):1805-1809. Available from: http://iovs.arvojournals.org/article.aspx?doi=10.1167/iovs.13-13264 doi: 10.1167/iovs.13-13264.

21. Amini R, Whitcomb JE, Al-Qaisi MK, Akkin T, Jouzdani S, Dorairaj S, et al. The posterior location of the dilator muscle induces anterior iris bowing during dilation, even in the absence of pupillary block. Invest Ophthalmol Vis Sci 2012;53(3):1188-1194. Available from: http://iovs.arvojournals.org/article.aspx?doi=10.1167/iovs.11-8408 doi: 10.1167/iovs.11-8408.

22. Amini R, Jouzdani S, Barocas VH. Increased iris–lens contact following spontaneous blinking: Mathematical modeling. Journal of Biomechanics 2012;45(13):2293-2296. Available from: http://linkinghub.elsevier.com/retrieve/pii/S0021929012003508 doi: 10.1016/j.jbiomech.2012.06.018.

23. Amini R, Barocas VH. Reverse pupillary block slows iris contour recovery from corneoscleral indentation. J Biomech Eng 2010;132(7):71010. Available from: http://Biomechanical.asmedigitalcollection.asme.org/article.aspx?articleid=1429231 doi: 10.1115/1.4001256.

24. Jouzdani S, Amini R, Barocas VH. Contribution of different anatomical and physiologic factors to iris contour and anterior chamber angle changes during pupil dilation: theoretical analysis. Invest Ophthalmol Vis Sci 2013;54(4):2977-2984. Available from: http://iovs.arvojournals.org/article.aspx?doi=10.1167/iovs.12-10748 doi: 10.1167/iovs.12-10748.

25. Storn R, Price K. Differential evolution–a simple and efficient heuristic for global optimization over continuous spaces. J Global Optimiz 1997;11(4):341-359.

26. Ohio Supercomputer Center. Oakley supercomputer (Columbus, OH). 2012.

27. Johnson M, Schuman JS, Kagemann L. Trabecular meshwork stiffness in the living human eye. Invest Ophthalmol Vis Sci 2015;56(7):3541-3541.

28. Camras LJ, Stamer WD, Epstein D, Gonzalez P, Yuan F. Effects of trabecular meshwork stiffness on outflow. Invest Ophthalmol Vis Sci 2012;53(9):5242-5250. Available from: http://iovs.arvojournals.org/article.aspx?doi=10.1167/iovs.12-9825 doi: 10.1167/iovs.12-9825.

29. Wang K, Read AT, Sulchek T, Ethier CR. Trabecular meshwork stiffness in glaucoma. Exp Eye Res. May 2017;158: 3-12.https://doi.org/10.1016/j.exer.2016.07.011

30. Simon B, Kaufmann M, McAfee M, Baldwin A. Finite element models for arterial wall mechanics. J Biomech Eng-T ASME 1993;115(4B):489-489. Available from: http://Biomechanical.asmedigitalcollection.asme.org/article.aspx?articleid=1399604 doi: 10.1115/1.2895529.

31. Soltz MA, Ateshian GA. A conewise linear elasticity mixture model for the analysis of tension-compression nonlinearity in articular cartilage. J Biomech Eng-T ASME 2000;122(6):576-586.

32. Powell TA, Amini R, Oltean A, Barnett VA, Dorfman KD, Segal Y, et al. Elasticity of the porcine lens capsule as measured by osmotic swelling. J Biomech Eng 2010;132(9):91008. Available from: http://Biomechanical.asmedigitalcollection.asme.org/article.aspx?articleid=1426860 doi: 10.1115/1.4002024.

33. Nagel TM, Hadi MF, Claeson AA, Nuckley DJ, Barocas VH. Combining displacement field and grip force information to determine mechanical properties of planar tissue with complicated geometry. J Biomech Eng 2014;136(11):114501. Available from: http://biomechanical.asmedigitalcollection.asme.org/article.aspx?doi=10.1115/1.4028193 doi: 10.1115/1.4028193.